Data report: characterization of sulfide minerals from gabbroic and ultramafic rocks by electron microscopy[1]

D.J. Miller,[2] T. Eisenbach,[2] and Z.P. Luo[3]

Chapter contents

[1] Miller, D.J., Eisenbach, T., and Luo, Z.P., 2009. Data report: characterization of sulfide minerals from gabbroic and ultramafic rocks by electron microscopy. *In* Blackman, D.K., Ildefonse, B., John, B.E., Ohara, Y., Miller, D.J., MacLeod, C.J., and the Expedition 304/305 Scientists, *Proc. IODP,* 304/305: College Station, TX (Integrated Ocean Drilling Program Management International, Inc.). doi:10.2204/iodp.proc.304305.203.2009
[2] Integrated Ocean Drilling Program, Texas A&M University, 1000 Discovery Drive, College Station TX 77845-9547, USA. Correspondence author: **miller@iodp.tamu.edu**
[3] Microscopy and Imaging Center, Biological Sciences Building West, Texas A&M University, College Station TX 77843-2257, USA.

Abstract

This objective of this research was to investigate the potential of using transmission electron microscopy (TEM) to determine sulfide mineral speciation in gabbroic rocks from Atlantis Massif, the site of Integrated Ocean Drilling Program Expedition 304/305. The method takes advantage of TEM analysis techniques and proved successful in sulfide mineral identification. TEM can provide imaging of the sample morphology, crystal structure through the electron diffraction, and chemical compositional information through X-ray energy dispersive spectroscopy. Electron probe microanalysis was also used to determine the chemical composition.

Introduction

Integrated Ocean Drilling Program (IODP) Expedition 304/305 at Atlantis Massif, 30°N on the Mid-Atlantic Ridge (MAR) (Fig. **F1**) comprised a coordinated, dual-expedition drilling program aimed at investigating oceanic core complex (OCC) formation and the exposure of ultramafic rocks in young oceanic lithosphere. One of the scientific objectives of this drilling program is to investigate the role of magmatism in the development of OCCs. Whereas precruise submersible and geophysical surveys suggested the potential of recovering substantial amounts of serpentinized peridotite and possibly fresh residual mantle, coring on the central dome of the massif returned a 1.4 km thick section of plutonic mafic rock with only a thin (<150 m) interval of ultramafic or near-ultramafic composition rocks of indeterminate origin. Strikingly, despite the abundance of serpentinized peridotite in dredge hauls and submersible surveys from OCCs, in each instance where scientific ocean drilling has penetrated one of these core complexes (Mid-Atlantic Ridge Kane Fracture Zone, Atlantis Bank, 15°20′N on the MAR, and now Atlantis Massif) virtually the only rock type recovered is gabbro (Ildefonse et al., 2006). Therefore, unraveling the magmatic and alteration history of these plutonic sequences is essential to understanding OCC formation.

Herein we report the results of a new study that was envisioned to develop a method for characterization of the primary sulfide mineral assemblage present in the gabbroic and ultramafic rocks from Atlantis Massif. The abundance and composition of primary sulfide minerals is an integral part of a larger scope collaborative effort aimed at using the entire sulfide mineral assemblage in these

doi:10.2204/iodp.proc.304305.203.2009

gabbroic rocks to estimate sulfur and oxygen fugacity in the magma during crystallization. These estimates can be compared with oxygen fugacities calculated from oxide mineral compositions and ultimately provide constraints on oxide-silicate relationships used to determine temperatures and pressures of equilibration during the crystallization of the gabbros.

Characterization of sulfide mineral assemblages has historically been accomplished through reflected light microscopic techniques. More recently, researchers have adopted geochemical analysis by electron microprobe as a common analytical technique. As a result of the combination of utilization of the electron microprobe as an analytical tool and the fact that petrographic analysis of silicate phases does not require reflected light, the skills required to master sulfide mineral identification are commonly underdeveloped in students. We envisioned a project that would attempt to utilize the transmission electron microscopy (TEM) skills of a researcher who lacked experience in standard petrographic techniques to characterize sulfide minerals. TEM images samples at very high resolution (typically several angstroms), providing crystal structure details through electron diffraction. TEM can also provide chemical composition using X-ray energy dispersive spectroscopy (EDS).

Geologic background

Drilling in Hole U1309D penetrated >1.4 km with >75% recovery, comparable to recovery from the previous most successful penetration into oceanic lithosphere in Ocean Drilling Program (ODP) Leg 118 Hole 735B on the Southwest Indian Ridge. Despite high seismic velocities interpreted to possibly represent residual mantle at relatively shallow depth, the 1.4 km section appears to be wholly igneous crust with little evidence of ductile deformation and brittle deformation confined to a few intervals less than a couple of meters thick.

Major plutonic lithologies recovered are, in decreasing abundance, gabbro, olivine gabbro, troctolite, oxide-bearing gabbro, oxide gabbro, and oxide- and olivine-bearing gabbro. The gabbroic rocks have compositions that are among the most primitive sampled along the MAR, as reflected in bulk Mg numbers ranging from ~67 to 90 (see the **"Expedition 304/305 summary"** chapter). At least two generations of sulfide mineralization have been identified during shipboard and postcruise reconnaissance examination. Based on optical properties, the primary sulfide mineral assemblage includes at least pyrrhotite, pentlandite, and chalcopyrite, indicative of relatively oxygenated and sulfur-rich conditions. These phases occur as armored inclusions in silicate phases and as intergranular crystals. Secondary sulfides, which occur in veins and as inclusions in alteration phases, include pyrite and tentatively identified tochilinite and awaruite, indicative of highly oxygen and sulfur depleted conditions. In some cases, both primary and secondary assemblages occur in the same thin section, attesting to the complex history of sulfide mineralization in the section.

Method development

Attempts at TEM analysis of standard petrographic thin sections proved unfruitful, as the sulfide mineral grains are typically small (commonly <50 µm) and the total abundance of sulfide mineral is commonly <1 mod%. Eventually, we settled on grain mount preparations derived from pulverizing the samples to <1 mm grain size and then deriving a heavy mineral separate using a dense sodium polytungstate solution.

After the sulfides were separated from the bulk material, they were mixed in ethanol solutions and deposited on Cu grids, which were previously glow discharged in order to achieve better dispersions. TEM measurements were carried out using a JEOL 2010 TEM system at a working voltage of 200 kV. All imaging magnifications were calibrated using the standards of SiC lattice fringes (Luo, 2006) for high magnifications and commercial cross-line grating replica for low magnifications. EDS, which was used to determine chemical composition, was done using an Oxford Instruments EDS detector with an INCA energy platform. Electron micrographs were digitalized using an Epson (Long Beach, CA) Projection 3200 scanner at 1200 dpi.

Reflected light petrography and electron microprobe analyses were performed on representative samples of the various major lithologies for comparison with TEM results. Analyses of sulfide minerals were performed using the CAMECA SX-50 electron microprobe. Analyses were performed using a 50 nA beam current, an accelerating voltage of 15 keV, and a 1 µm beam. Count times range from 20 to 40 s. Standards used included pyrite (S and Fe); sphalerite (Zn); and pure Co, Ni, and Cu wire.

Results

Figure **F2A** is a TEM image of sulfide mineral grains. These particles have sharp, regular faces and are several micrometers in breadth. The selected area electron diffraction (SAED) patterns (Fig. **F2B, F2C**) from these particles, along two different zone axes of [011]

and [012], show that these grains are crystalline with a primitive cubic structure (a = 0.54166 nm) and a space group of $Pa\overline{3}$ (#205). Higher magnification images are shown in Figure **F3A,** which is further magnified in Figure **F3B** from the framed area in Figure **F3A,** where lattice fringes (also potentially useful for mineral identification) are visible. The structure and space group are consistent with the mineral pyrite.

Chalcopyrite grains are shown in a TEM image in Figure **F4A.** The particles are micrometer scale, with regular shape and sharp crystal faces where unbroken. The SAED patterns from these particles (Fig. **F4B, F4C**) reveal that they have a tetragonal structure (a = 0.5289 nm, c = 1.0423 nm) and a space group of $I\overline{4}\ 2d$ (#122). Figure **F4B** is along the [001] zone axis of the tetragonal structure, where the reflection spots are in a regular square shape consistent with tetragonal structure along this axis. Figure **F5A** is an image in higher magnification, the framed area of which is further magnified in Figure **F5B,** imaging lattice fringes.

In order to verify the chemical composition of grains, we performed EDS on the samples. Figure **F6A** shows an EDS spectrum from the pyrite sample. The sample contains S and Fe; C is from the support carbon film of the grid and the low Cu peak is from the Cu grids. Future studies could employ Au grids to alleviate the Cu signal. A quantitative analysis shows the composition of Fe:S = 31.2:68.8 in atomic ratio, consistent with the stoichiometry of FeS_2. Alternatively, the EDS spectra from the chalcopyrite (Fig. **F5B**) clearly shows higher Cu content in addition to Fe and S. The quantitative analysis of the spectra reveals that the composition of these grains is Cu:Fe:S = 30.2:32.3:37.5. Although the stoichiometry of $CuFeS_2$ is Cu:Fe = 1:1, we assign the discrepancy to less than ideal accuracy of S determination EDS with TEM.

Although a detailed analysis has not been part of this trial, the following observations of primary sulfide mineralogy hold based on examination of 24 thin sections and sulfide mineral analysis of 9 thin sections (Table **T1**). Two troctolites were examined, one from fairly shallow in the hole (Sample 304-U1309D-60R-3, 59–62 cm) and one from deep in the hole (Sample 305-U1309D-233R-2, 137–140 cm). Despite similar primary mineralogies (75% olivine, 25% plagioclase), the sample from the upper ultramafic horizon is significantly more altered (80% versus 20%), and the sulfide minerals are heazelwoodite and polydimite in the upper sample (Section 304-U1309D-60R-3) and pyrrhotite and mackinawite in the sample from the deeper interval (Section 305-U1309D-233R-2). The olivine gabbros and olivine-bearing gabbros have a consistent sulfide mineral assemblage of pyrrhotite > chalcopyrite > pentlandite, and pyrite is ubiquitous but in variable abundance and is likely mostly secondary. Pentlandite containing as much as 2 wt% Co occurs as flamelike exsolution features and as granular to subrounded grains near the margins of pyrrhotite. Chalcopyrite is most commonly manifested as blade-shaped inclusions in pyrrhotite. Gabbro samples have a similar pyrrhotite > chalcopyrite > pentlandite sulfide mineral assemblage, but several samples also include rare sphalerite. The only sulfide minerals found in oxide-bearing gabbros were pyrrhotite and chalcopyrite, but only a few samples of this lithology were examined so the absence of pentlandite might not be significant. Oxide gabbros contain pyrrhotite > chalcopyrite > pentlandite. The pentlandite in the oxide gabbros contains as much as 12 wt% Co.

Discussion

This project was initiated as part of a collaborative investigation among shipboard science party members from Expedition 304/305. The overall objective of the research plan is to use primary and secondary sulfide minerals to map changes in sulfur and oxygen fugacity during hydrothermal alteration of the plutonic foundation of the ocean crust. Specifically, our group set out to document the composition and diversity of primary sulfide minerals providing the starting end-member for studies evaluating the composition and evolutions of fluids migrating through the massif and contributing to alteration of the rocks. For example, Miller (2007) shows that the sulfide mineral assemblage at ODP Site 1268 (millerite + polydymite in near-surface rocks, progressing in deeper rocks to assemblages including pyrrhotite and then pentlandite) records fluids seeping down from the seafloor, becoming progressively less oxygenated and less sulfur-rich as they react with the host rock and precipitate sulfide minerals.

Classically trained sulfide petrologists can, through years of practice and likely an inherently acute sense of subtle differences in color, reflectivity, and hardness, recognize sulfide species in reflected light. It is rare to find undergraduate or junior graduate students with this talent fully developed. In our case, we were intrigued by the hypothesis that someone without the benefits of traditional reflected light petrography education and practice might be able identify sulfide minerals from these ocean crust rocks using TEM. We hoped to take advantage of the advanced facilities in the Texas A&M University Microscopy and Imaging Center to test this hypothesis,

employing a graduate student with TEM experience but no previous opportunity to work with natural sulfide-bearing materials.

Obviously, we had no doubt that TEM could be used to identify sulfide minerals, our purpose was to assess the process to see how sulfide mineral characterization with the TEM compared and contrasted with more traditional techniques.

In summary, by taking advantage of TEM analyses, we are satisfied that the method represents a robust approach to documenting the composition and diversity of sulfide minerals in gabbroic and ultramafic rocks, particularly when lacking experience in more traditional analytical techniques. As demonstrated in this project, with appropriate sample preparation, TEM analysis provides details regarding sulfide mineral crystal structure using electron diffraction and chemical composition from EDS. TEM analysis of sulfide minerals is broadly applicable to any host rock and may have specific interest for geologists and geochemists interested in serpentinization and/or hydrothermal mineralization. Although TEM operation and data interpretation require extensive experience, we surmise that this method might be used as an adjunct to standard petrographic and geochemical analysis techniques for sulfide minerals in oceanic crustal rocks.

Acknowledgments

This research used samples provided by the Integrated Ocean Drilling Program (IODP). Funding was provided to D.J. Miller by the United States Science Support Program. The authors acknowledge the contributions of Yaz Ohara and an anonymous reviewer to this manuscript.

References

Blackman, D.K., Ildefonse, B., John, B.E., MacLeod, C.J., Ohara, Y., Miller, D.J., and the Expedition 304/305 Project Team, 2004. Oceanic core complex formation, Atlantis Massif, Mid-Atlantic Ridge: drilling into the footwall and hanging wall of a tectonic exposure of deep, young oceanic lithosphere to study deformation, alteration, and melt generation. *IODP Sci. Prosp.,* 304/305. **doi:10.2204/iodp.sp.304305.2004**

Ildefonse, B., Blackman, D.K., John, B.E., Ohara, Y., Miller, D.J., MacLeod, C.J., and Integrated Ocean Drilling Expeditions 304/305 Science Party, 2006. Oceanic core complexes and crustal accretion at slow-spreading ridges. *Geology,* 35(7):623–626. **doi:10.1130/G23531A.1**

Luo, Z.P. 2006. Crystallography of $SiC/MgAl_2O_4/Al$ interfaces in a pre-oxided SiC reinforced SiC/Al composite–Dedicated to Professor H. Hashimoto on the occasion of his 80th birthday. *Acta Mater.,* 54(1):47–58. **doi:10.1016/j.actamat.2005.08.022**

Miller, D.J., 2007. Sulfide mineralization at Site 1268, Mid-Atlantic Ridge, Ocean Drilling Program Leg 209. *In* Kelemen, P.B., Kikawa, E., and Miller, D.J. (Eds.), *Proc. ODP, Sci. Results,* 209: College Station, TX (Ocean Drilling Program), 1–18. **doi:10.2973/odp.proc.sr.209.004.2007**

Initial receipt: 9 May 2008
Acceptance: 16 October 2008
Publication: 22 January 2009
MS 304305-203

Figure F1. A. Mid-Atlantic Ridge bathymetry (base image from www.ngdc.noaa.gov/mgg/image/2minrelief.html). **B.** Perspective view of Atlantis Massif and location of Site U1309. Base map modified from Blackman et al. (2004).

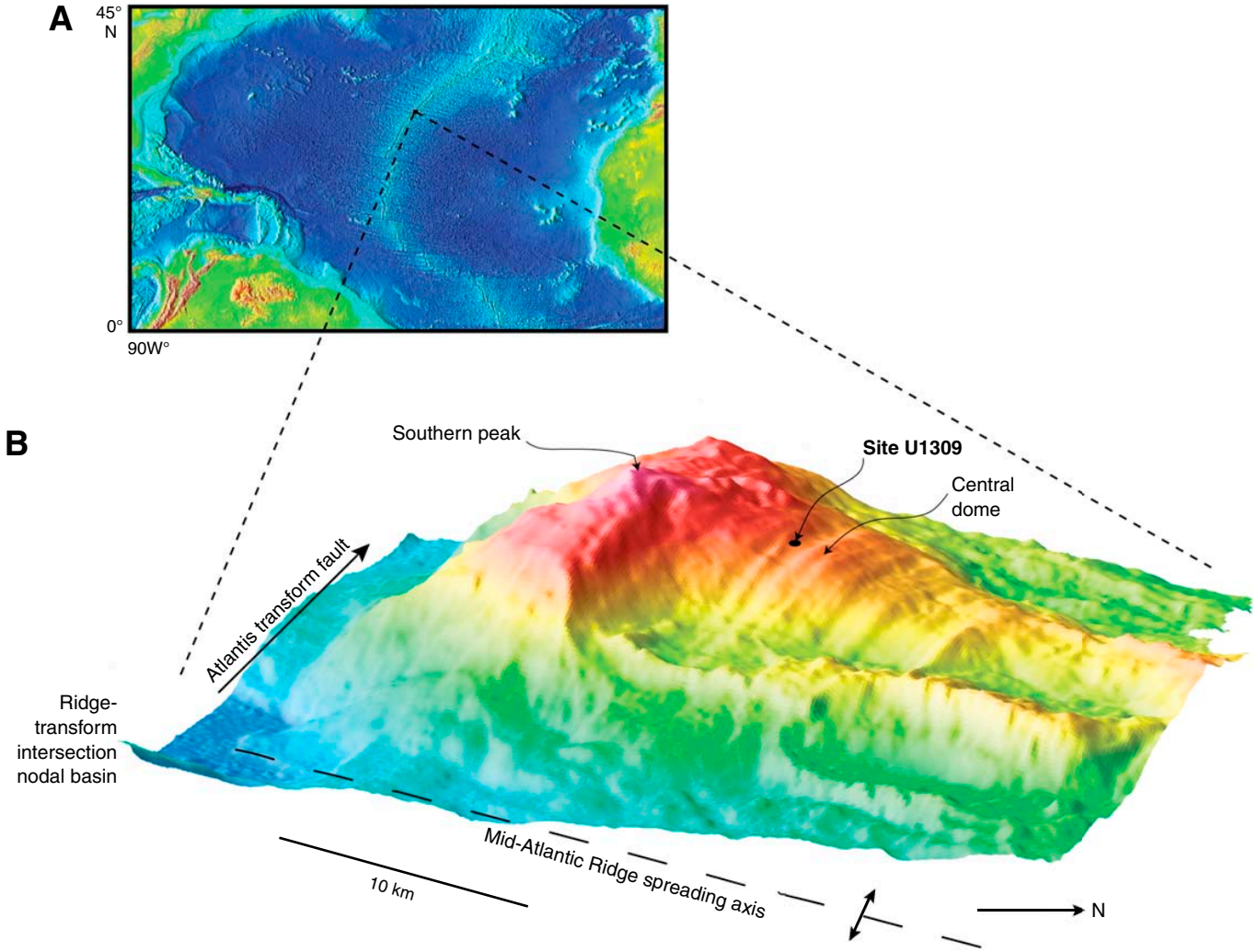

Figure F2. A. TEM photomicrograph of pyrite grains. **B, C.** Selected area electron diffraction patterns indicate simple cubic structure.

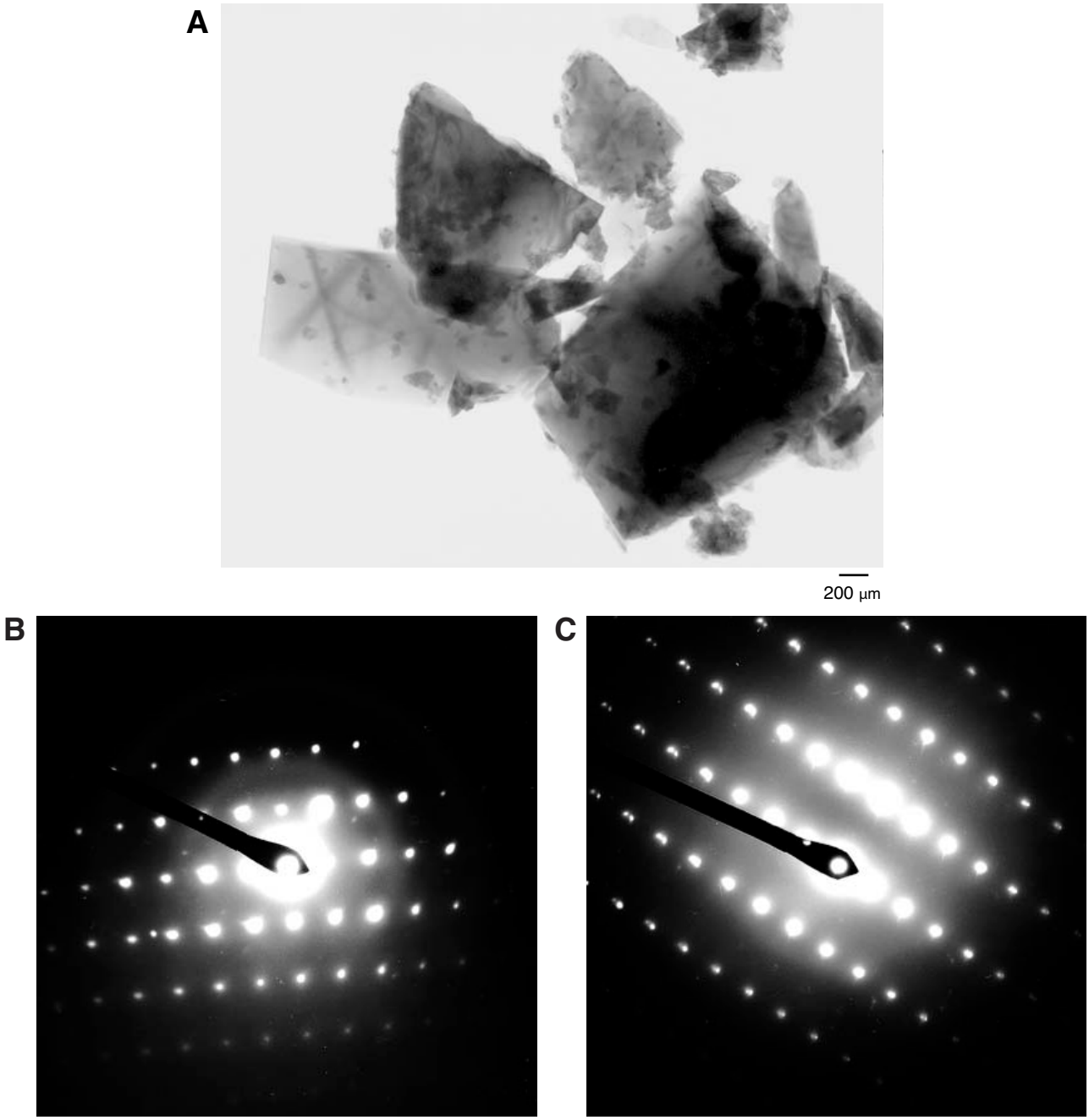

Figure F3. A. High-magnification TEM photomicrograph. **B.** Field of view (0.025 µm) from A showing lattice fringe structure of pyrite.

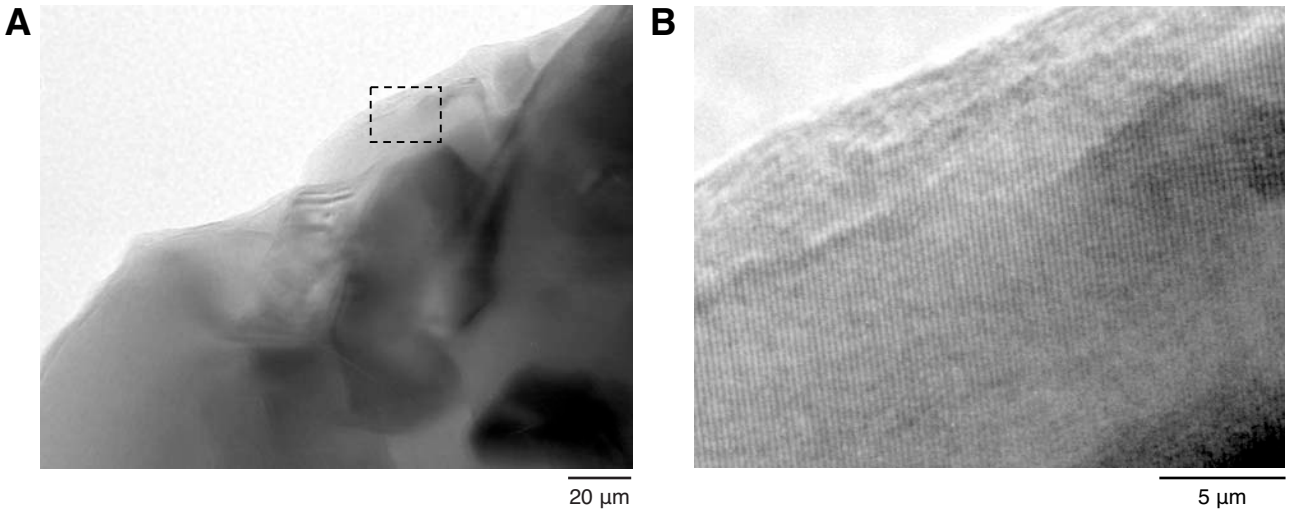

Figure F4. A. TEM photomicrograph of chalcopyrite grains. **B, C.** Selected area electron diffraction patterns indicate tetragonal structure.

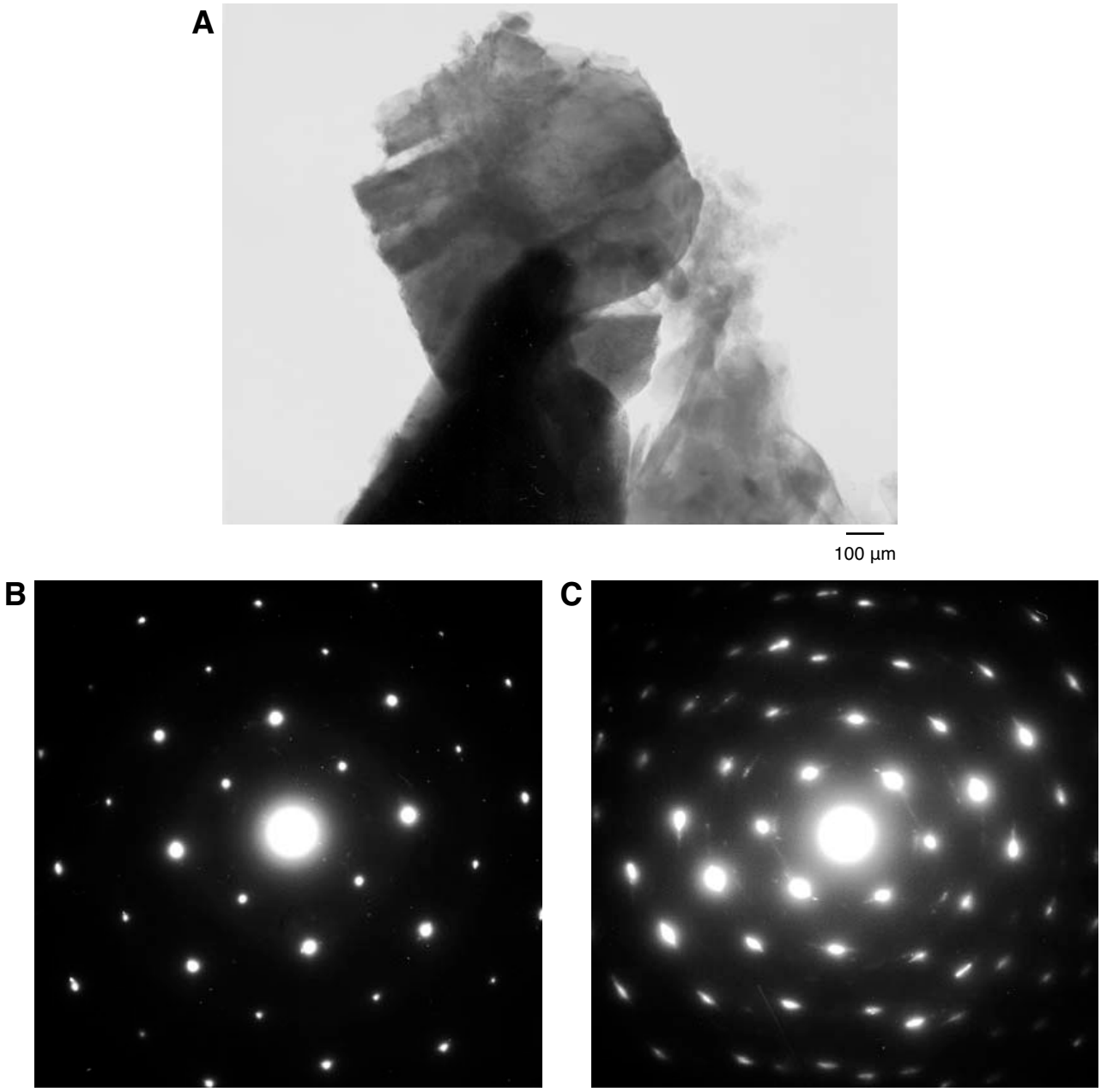

Figure F5. A. High-magnification TEM photomicrograph. **B.** Field of view (0.020 µm) from A imaging lattice fringes.

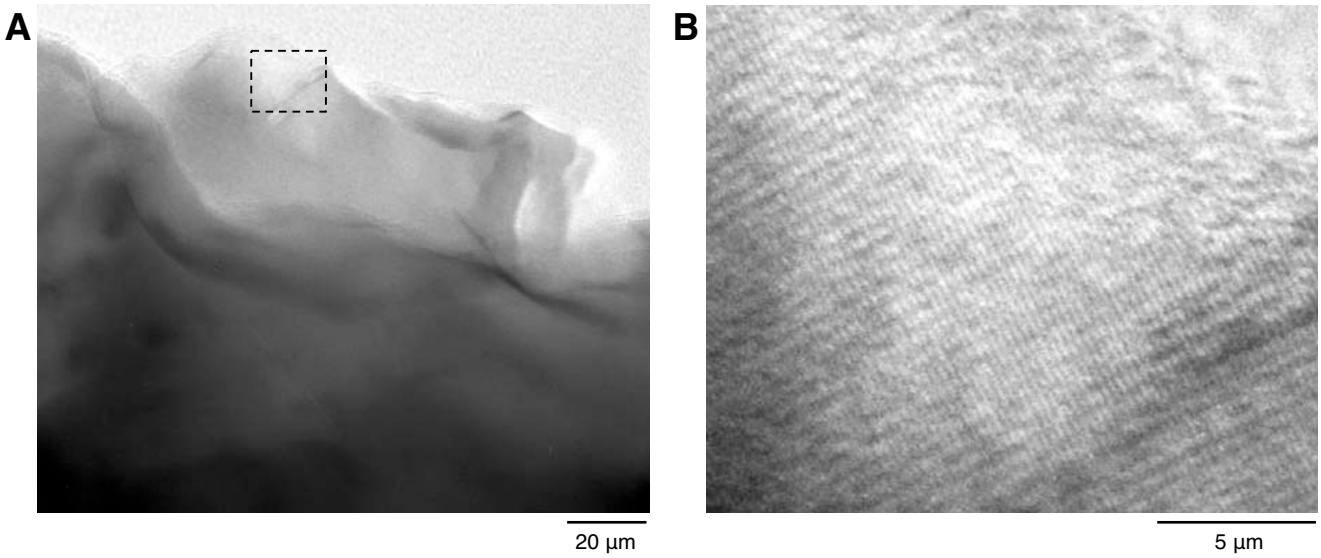

Figure F6. A. Energy dispersive spectra of pyrite grain. Small Cu peaks are caused by either sample or trace system contamination. **B.** Energy dispersive spectra of chalcopyrite sample.

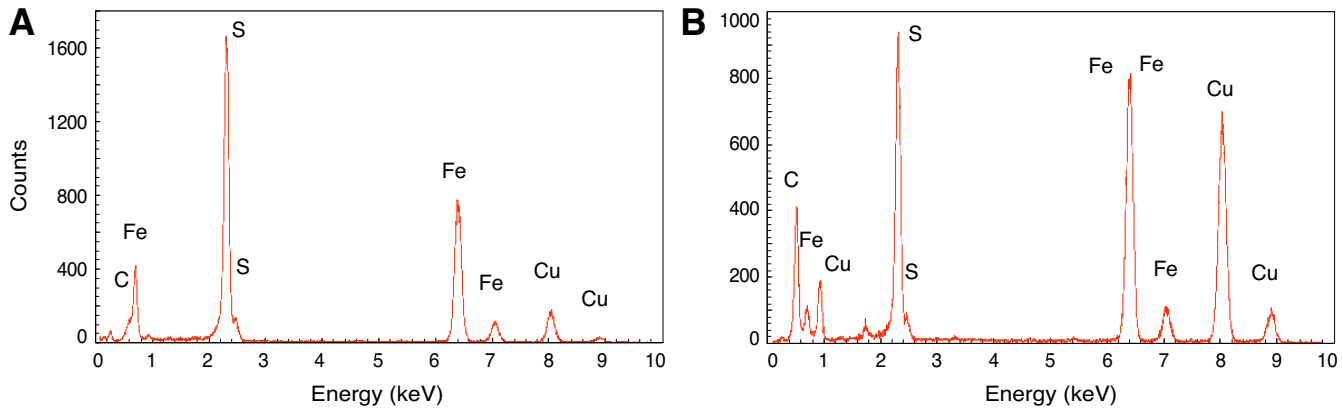

Table T1. Sulfide mineral electron microprobe analyses. (See table notes.)

Core, section, interval (cm)	Lithology	Depth (mbsf)	Major elements (wt%)						Mineral component
			S	Fe	Ni	Cu	Co	Zn	
304-U1309D-									
60R-3, 59–62	Altered troctolite	313.38	38.20	2.40	57.20	1.67	<0.05	ND	Polydimite
			27.30	1.40	73.30	0.09	<0.05	ND	Heazelwoodite
305-U1309D-									
233R-2, 137–140	Troctolite	1122.77	36.40	62.30	ND	ND	ND	ND	Pyrrhotite
			33.40	46.80	16.10	1.85	<0.05	ND	Mackinawite
212R-1, 108–111	Olivine gabbro	1021.11	38.60	59.70	0.50	0.05	ND	ND	Pyrrhotite
			35.20	29.90	0.10	33.52	<0.05	ND	Chalcopyrite
			34.00	32.30	31.60	0.09	1.92	ND	Pentlandite
227R-2, 13–16	Olivine gabbro	1093.56	36.40	62.30	ND	ND	ND	ND	Pyrrhotite
			34.90	32.40	0.70	32.35	ND	ND	Chalcopyrite
			31.40	27.70	31.50	4.10	1.57	ND	Pentlandite
268R-2, 49–52	Olivine gabbro	1289.72	37.70	60.90	0.40	<0.05	ND	<0.05	Pyrrhotite
			34.90	30.70	0.20	33.06	ND	0.08	Chalcopyrite
			33.60	35.10	29.10	0.14	2.09	<0.05	Pentlandite
208R-2, 83–86	Olivine-bearing gabbro	1002.91	38.40	60.00	0.20	ND	ND	ND	Pyrrhotite
			35.20	29.70	ND	33.62	ND	ND	Chalcopyrite
			33.70	33.60	30.80	0.01	2.09	ND	Pentlandite
223R-4, 11–14	Gabbro	1076.76	38.10	61.10	0.40	<0.05	0.00	56.20	Pyrrhotite
			35.00	30.30	ND	34.22	0.00	ND	Chalcopyrite
			33.60	33.00	31.10	0.13	2.38	0.49	Pentlandite
			33.90	9.00	0.10	0.49	0.10	56.20	Sphalerite
262R-1, 27–30	Oxide-bearing gabbro	1259.37	37.60	60.60	0.30	<0.05	ND	ND	Pyrrhotite
			34.90	30.50	0.10	32.95	<0.05	0.07	Chalcopyrite
265R-2, 100–103	Oxide gabbro	1275.95	38.00	60.50	0.30	<0.05	0.07	ND	Pyrrhotite
			34.90	30.50	0.10	32.95	<0.05	0.07	Chalcopyrite
			33.10	28.90	24.70	0.07	12.57	ND	Pentlandite

Notes: Average of 3–10 analyses. ND = not detected.